The chromatin remodeler RSC prevents ectopic CENP-A propagation into pericentromeric heterochromatin at the chromatin boundary

Satoru Tsunemine[1,2], Hiromi Nakagawa[3], Yutaka Suzuki[4] and Yota Murakami [1,*]

[1]Laboratory of Bioorganic Chemistry, Department of Chemistry, Faculty of Science, Hokkaido University, Sapporo 060-0810, Japan, [2]Laboratory of Cell Regulation, Graduate School of Biostudies, Kyoto University, Kyoto 606-8501, Japan, [3]Laboratory of Cell Regulation, Department of Viral Oncology, Institute for Virus Research, Kyoto University, Kyoto 606-8507, Japan and [4]Department of Computational Biology and Medical Science, Graduate School of Frontier Sciences, University of Tokyo, Kashiwa 277-8562, Japan

ABSTRACT

Centromeres of most eukaryotes consist of two distinct chromatin domains: a kinetochore domain, identified by the histone H3 variant, CENP-A, and a heterochromatic domain. How these two domains are separated is unclear. Here, we show that, in *Schizosaccharomyces pombe*, mutation of the chromatin remodeler RSC induced CENP-A^{Cnp1} misloading at pericentromeric heterochromatin, resulting in the mis-assembly of kinetochore proteins and a defect in chromosome segregation. We find that RSC functions at the kinetochore boundary to prevent CENP-A^{Cnp1} from spreading into neighbouring heterochromatin, where deacetylated histones provide an ideal environment for the spread of CENP-A^{Cnp1}. In addition, we show that RSC decompacts the chromatin structure at this boundary, and propose that this RSC-directed chromatin decompaction prevents mis-propagation of CENP-A^{Cnp1} into pericentromeric heterochromatin. Our study provides an insight into how the distribution of distinct chromatin domains is established and maintained.

GRAPHICAL ABSTRACT
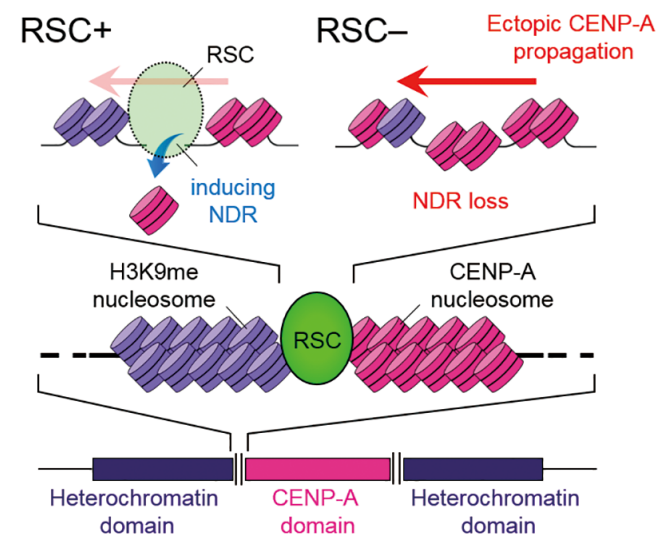
INTRODUCTION

Centromeres have a distinctive chromatin structure and a unique function in the genome; it marks the region of the chromosome upon which the kinetochore forms, a process that is crucial for faithful chromosome segregation. Nucleosomes at the centromere contain a centromere-specific variant of histone H3, CENP-A (1) and these CENP-A–containing nucleosomes provide a platform for kinetochore assembly (2). Domains containing these CENP-A nucleosomes usually associate with heterochromatin, which is defined by the presence of histone H3 methylated at Lys9 (H3K9me) and its associated binding protein, heterochromatin protein 1 (HP1). Heterochromatin associated with centromeres is thought to contain an inner kinetochore

*To whom correspondence should be addressed. Tel: +81 11 706 3813; Email: yota@sci.hokudai.ac.jp
Present address: Hiromi Nakagawa, Department of Comprehensive Metabology, Kanazawa University Graduate School of Medical Sciences, Kanazawa, Ishikawa 920-8641, Japan.

structure important for centromeric sister chromatid cohesion (3). In most eukaryotes, each chromosome has a single centromere, the position and size of which is epigenetically controlled (1). Mis-control of centromere positioning or size leads to chromosome instability. Accordingly, maintenance of faithful CENP-A deposition at centromeric regions is critically important for genome integrity. While previous studies have described a model for CENP-A deposition (4), the regulatory mechanisms required for regional propagation of the CENP-A chromatin domain remain poorly understood.

One key chromatin regulatory mechanism is the alteration of nucleosome positioning by chromatin remodelers. Multiple chromatin remodelers, including SWI/SNF, INO80 and SWR, are conserved from yeast to humans. While each remodeler plays a distinct role in nuclear events, the function of these complexes often overlap (5). In budding yeast, an abundant and essential chromatin remodeling complex RSC, a member of the SWI/SNF complex, plays important biological roles, such as transcriptional control, kinetochore function, sister chromatid cohesion, and DNA repair (6–9), which appear to be conserved in fission yeast (10–12). In addition, yeast RSC generates nucleosome-depleted regions (NDR), especially around transcription start sites, which is implicated in transcriptional regulation (13–17). Budding yeast RSC is shown to have nucleosome sliding and eviction activity *in vitro* (18,19), but how these biochemical activities contribute to the functions of RSC is unclear.

In most eukaryote, some chromatin remodelers are responsible for a faithful CENP-A deposition in centromere, whereas others are involved in the prevention of inappropriate propagation of CENP-A. The ATP-dependent SWI/SNF chromatin remodeling complex, for example, plays a role in maintaining CENP-A^{Cse4} distribution at budding yeast centromeres, which are small and contain no centromeric heterochromatin (20). The SWI/SNF complex is implicated in the maintenance of CENP-A^{Cse4} in the centromeric region: loss of SWI/SNF broadens the distribution of CENP-A^{Cse4} and decreases the nuclease sensitivity of hypersensitive sites flanking the centromeres, suggesting that the formation of hypersensitive sites is involved in the accurate distribution of CENP-A^{Cse4}. In *Drosophila*, a mutation of *CHRAC14*, a subunit of the chromatin accessibility complex (CHRAC) containing ISWI chromatin remodeler, causes a deficiency of DNA damage repair and ectopic CENP-A^{CID} deposition to the damaged sites, resulting in the formation of ectopic kinetochore, which suggests that CHRAC14 is involved in prevention of ectopic CENP-A^{CID} assembly (21). FACT and a subunit of the 19S proteasome prevent the ectopic localization of fission yeast CENP-A^{Cnp1} by a poorly understood mechanism (22,23). Interestingly, RSC was identified as a binding partner of Swi6, a fission yeast homologue of HP1 (heterochromatin protein 1), by mass spectrometry (24,25), and RSC localizes at the pericentromeric region (12). However, the role of RSC at pericentromeric heterochromatin is still unknown.

In this study, functional analysis of a mutant of a core RSC subunit in fission yeast, *sfh1*, reveals that Sfh1/RSC facilitates chromatin decompaction at the boundaries between CENP-A^{Cnp1} chromatin and heterochromatin, which may prevent ectopic CENP-A^{Cnp1} propagation into pericentromeric heterochromatin. Consistent with these findings, the insertion of a transcriptionally active gene that induces chromatin decompaction into the boundary can prevent the ectopic CENP-A^{Cnp1} mis-propagation over the boundary in the absence of Sfh1/RSC. We show that Sfh1/RSC is required to create a barrier capable of preventing CENP-A^{Cnp1} chromatin propagation into surrounding heterochromatic domains.

MATERIALS AND METHODS

Strains, media, and genetic procedures

All strains used in this study are listed in Supplementary Table S1. The media and genetic procedures used in this study were described previously (26). Most experiments were conducted in yeast extract with supplements (YES) media or Edinburgh minimal medium with supplements (EMMS) at 30°C. Temperatures were shifted to 36°C for 8 h to inactivate temperature-sensitive Sfh1, Snf21 and Sfc3. Deletion and tagging of target genes were performed as previously described (27).

Antibodies

Rabbit polyclonal antibodies against Cnp1 (28) and histone H3 (ab1791) were obtained from Abcam. Mouse monoclonal antibodies against H3K9me (29), H3K14ac (7G8) and Pol2 CTD (4H8) were obtained from Millipore. Mouse monoclonal antibodies against epitope tags, Myc (4A6/Millipore) and FLAG (M2/Sigma) were used for ChIP assays and immunoblotting.

Microscopy

Fluorescent images were taken with ZEISS Axio Imager M1 (CARL ZEISS). Measurements of GFP-Cnp1 and Sad1-DsRed foci size were performed using ImageJ software. Indirect immunofluorescence analysis was performed essentially as previously described (30,31), except that cells were incubated with primary antibodies at room temperature for 3 h each. Anti-TAT1 was used as primary antibody, and a rabbit IgG antibody conjugated to Alexa Fluor 488 (Invitrogen) was used as the secondary antibody.

Micrococcal nuclease analysis of chromatin structure

Micrococcal nuclease (MNase) digestion of genomic DNA was performed as previously described (32), with some modifications. The cell walls of growing cells fixed with 1% formaldehyde were digested with 0.5 mg/ml Zymolyase 20T in sorbitol/Tris buffer. Spheroplasts were treated for 20 min at 37°C with 10 U/ml MNase (Takara Bio) in NP buffer containing 1 mM 2-mercaptoethanol and 0.5 mM spermidine. After treatment with RNase A and proteinase K, residual DNA in the supernatant was purified by phenol/chloroform extraction. Mononucleosomal DNA was separated by 2% agarose gel electrophoresis, purified, and subjected to quantitative PCR (qPCR). MNase protection was normalized to the TTS of *act1*, which is a region of constitutive-NDR (33).

ChIP analysis

2×10^8 cells growing exponentially in YES were fixed with 1% formaldehyde (Nacalai Tesque) for 20 min at 30°C. After fixation was quenched with 150 mM glycine, cells were harvested and washed twice with Lysis Buffer (50 mM HEPES [pH 7.5], 1 mM EDTA, 1% Triton X-100, and 0.1% Na-deoxycholate). The cell pellet was re-suspended in lysis buffer containing 1 mM PMSF and a protease inhibitor cocktail, and homogenized with a bead shocker (Yasui Kikai) 30 times for 60 s each at 4°C. Lysis buffer containing 1 mM PMSF, and a protease inhibitor cocktail was added to the resulting cell extracts to 2 ml. Cell extracts were sonicated for 240 sec using a New Bioruptor (CosmoBio) set at level 'H', centrifuged at 15 000 rpm for 15 min at 4°C, and the resultant supernatant was used as the input fraction.

The input fraction was subject to immunoprecipitation with secondary antibody-conjugated magnetic beads (Invitrogen) preincubated with antibody against the target protein or epitope. Beads were washed with Lysis Buffer and incubated for 2 h with cell extract at 4°C. After immunoprecipitation, the beads were washed twice each with lysis buffer; lysis/500 mM NaCl buffer containing 1 mM PMSF and protease inhibitor cocktail; wash/LiCl buffer (10 mM Tris [pH 8.0], 250 mM LiCl, 0.5% NP-40 and 0.5% Na-deoxycholate), containing 1 mM PMSF and protease inhibitor cocktail; and TE buffer (10 mM Tris [pH 8.0], 1 mM EDTA). The beads were then suspended in TE buffer containing RNase A and incubated for 1 h at 37°C. Proteinase K (0.5 mg/ml) was added, and the mixture was incubated for an additional 1 h at 45°C. After reversal of crosslinks by incubation at 65°C, DNA was purified by phenol/chloroform extraction, and qPCR was performed.

Quantitative PCR

qPCR was performed in PCR reactions containing SYBR Dye on a Thermal Cycler Dice Real Time System (Takara Bio). Primers used are listed in Supplementary Table S2. In each graph showing qPCR results, error bars represent the standard error of the mean of biologically independent experiments ($n = 3$). All ChIP-qPCR enrichments except those for Snf21-myc and FLAG-Sfh1 were calculated as % DNA immunoprecipitated at the locus of interest relative to the corresponding input samples, and normalized to % DNA immunoprecipitated at the *act1+* locus, which is indicated as 'Fold enrichment over *act1*' in each plots. As for Snf21-myc and FLAG-Sfh1 (Figures 3F and 5E), we cannot use *act1+* locus as a reference because *sfh1-13* affect the localization of Sfh1 at this locus. Therefore, the calculated % DNA immunoprecipitated were normalized to that of no-tag control.

ChIP-sequencing (ChIP-seq) and next-generation sequencing (NGS)

Cells were cultured in 500 ml YES to a density of 1×10^7 cells/ml, and processed as described above for ChIP analysis. ChIP-seq samples for the Illumina platform were prepared according to the manufacturer's instructions. The libraries were sequenced on the Illumina HiSeq 2000 system (single-end, 36 bp). The sequenced reads were mapped onto the *S. pombe* reference genome (strain 972) using BWA (34), and then processed using SAMtools (35). For reads with multiple aligned location, we randomly assigned single locations. In the R-statistical environment (http://www.R-project.org), we calculated the IP/WCE ratio using wiggle format pileup files (step size: 10 bp) generated by MACS (36). The generated wig files was visualized by the Integrative Genomics Viewer (37). The experiments were not repeated.

RNA extraction and RT-PCR

Strains were cultured in 10 ml YES media to a density of 1×10^7 cells/ml, harvested by centrifugation, and washed with 10 ml PBS. The cell pellet was suspended in buffer containing 1% sodium dodecyl sulfate (SDS) and acid phenol. Total RNA was extracted using a freeze–thaw treatment: rapid freezing in liquid N_2 followed by 1 h incubation in a water bath at 65°C. RT-PCR was performed using Prime Script (Takara Bio).

RESULTS

The *sfh1-13* mutant is sensitive to CENP-A^{Cnp1} overexpression

RSC localizes at both the kinetochore domain and pericentromeric heterochromatin. Temperature-sensitive mutants of *sfh1* or *snf21*, core subunits of RSC, are sensitive to the microtubule-destabilizing drug thiabendazole (TBZ) and exhibit an elevated rate of minichromosome loss (11,12). Mutants that disrupt chromosome segregation are often hypersensitive to TBZ (38). In addition, a low concentration of TBZ enhanced the chromosome segregation defects of the temperature-sensitive *sfh1-13* mutant (Supplementary Figure S1A). These results suggest a role for RSC in accurate chromosome segregation, although the level of CENP-A^{Cnp1} at the central domain, and the amount of H3K9me at the pericentromeric domain, do not change in *sfh1-13* cells (12). Previous work has shown that mutations of the histone chaperon FACT and the 19S proteasome can cause inappropriate deposition of CENP-A^{Cnp1} at noncentromeric regions when CENP-A^{Cnp1} is overexpressed, leading to slow growth (22,23). We hypothesized that the *sfh1-13* mutation might also affect the dynamic properties of CENP-A^{Cnp1}, causing inappropriate deposition. Therefore, we used cells over-expressing CENP-A^{Cnp1} under the control of the thiamine-repressible *nmt3* and *nmt41* promoters, which express target genes at high and medium strength, respectively (39,40), to examine the effects of CENP-A^{Cnp1} overexpression on cell growth in wild-type and *sfh1-13* cells (Supplementary Figure S1B). The growth of the wild-type strain was not affected by CENP-A^{Cnp1} overexpressed from *nmt41* (*nmt41-cnp1*) at any temperature examined; however, the *sfh1-13* mutant strain exhibited a slow growth phenotype at 32°C upon *nmt41-cnp1* expression (*sfh1-13* at 32°C in the lower panel of Supplementary Figure S1B). CENP-A^{Cnp1} expression from the *nmt3* promoter (*nmt3-cnp1*), which induces a greater level of expression than *nmt41-cnp1*, led to growth defects in the wild-type strain at all temperatures examined, with increased sensitivity at

32°C and 36°C (upper panel, Supplementary Figure S1B). The *sfh1-13* mutation was synthetic lethal with *nmt3-cnp1* at 32°C (upper panel; Figure 1A), suggesting that Sfh1/RSC is involved with CENP-A^{Cnp1} dynamics. A previous study identified the mutations of SWI/SNF chromatin remodeling complex as the suppressor mutants for temperature-sensitive *mis18* and *mis19* mutants, which encode subunits of CENP-A^{Cnp1} recruiting complex, suggesting that this remodeler could counteracts the CENP-A^{Cnp1} recruiting machinery ([41]). However, deletion strains of two genes encoding SWI/SNF core components, *snf5* and *snf22*, did not exhibit sensitivity to CENP-A^{Cnp1} overexpression (Supplementary Figure S2A). Moreover, depletion of SWI/SNF-specific components does not increase TBZ sensitivity ([10]). These data suggest that RSC, but not SWI/SNF, plays a role in stabilizing CENP-A^{Cnp1}.

Sfh1/RSC prevents the spread of CENP-A^{Cnp1} into the pericentromeric heterochromatin domain

Since the sensitivity of FACT mutants to CENP-A^{Cnp1} overexpression is linked to the accumulation of CENP-A^{Cnp1} at non-centromeric locations ([22]), we speculated that loss of Sfh1 function may also allow the incorporation of CENP-A^{Cnp1} at non-centromeric locations. We therefore performed chromatin immunoprecipitation and high-throughput sequencing (ChIP-seq) with anti-CENP-A^{Cnp1} in wild-type and *sfh1-13* mutant cells to examine CENP-A^{Cnp1} loading. When CENP-A^{Cnp1} was expressed at wild-type levels, specific accumulation at pericentromeric heterochromatin domains of all centromeres (Figure 1A), but not at non-centromeric locations (Supplementary Figure S3), was observed in *sfh1-13* mutant cells, as verified by ChIP-quantitative PCR (ChIP-qPCR; Figure 1B). However, a mild effect on the localization of CENP-A^{Cnp1} at the central core region (*cnt*), compared with pericentromeric (*dg* and *dh*) regions, was detected (Figure 1A and B). Note that, in permissive temperature, the perturbation of CENP-A^{Cnp1} level at *dg/dh* region did not occur in *sfh1-13* cells (Supplementary Figure S4). Importantly, no significant difference in the level of Cnp1 protein or mRNA was seen in *sfh1-13* cells (Figure 1E). In addition, *sfh1-13* mutation does not affect the expression levels of CENP-A^{Cnp1} chromatin-related genes (Supplementary Figure S5). Furthermore, we observed ectopic CENP-A^{Cnp1} deposition at pericentromeric heterochromatin domains in *snf21-36* but not in *rsc1* and *rsc4* deletion mutants (Figure 1F). Snf21 is an ATPase containing a core subunit of RSC, while Rsc1 and Rsc4 are non-essential subunits of the same complex, and these results suggest that RSC remodeling activity is responsible for the preventing CENP-A^{Cnp1} loading at pericentromere. By contrast, deletion mutants of SWI/SNF components, *snf5Δ* and *snf22Δ*, did not exhibit an increase in the abundance of CENP-A^{Cnp1} at pericentromeric repeats (Supplementary Figure S2B).

It is possible that heterochromatin prevent CENP-A^{Cnp1} misloading and that the *sfh1-13* mutation alters the heterochromatin structure so that it fails to prevent CENP-A^{Cnp1} misloading. However, the *sfh1-13* mutation had only a mild influence on H3K9me levels (Figure 1C), as we reported previously ([12]). In addition, CENP-A^{Cnp1} did not accumulate at pericentromeric domains in *clr4Δ* cells, which completely lose their heterochromatin structure (Figure 1B and C), indicating that heterochromatin structure does not contribute to prevention of CENP-A^{Cnp1} misloading. The levels of histone H3 and H3K9me were slightly reduced at centromere in *sfh1-13* cells (Figure 1C and D), possibly indicating the replacement of histone H3 with CENP-A^{Cnp1} at these repeats in *sfh1-13* mutant cells. In contrast to pericentromeric heterochromatin, the incorporation of CENP-A^{Cnp1} at the mating locus and subtelomeric heterochromatin was not detected (Figure 1G), suggesting that CENP-A^{Cnp1} had spread from the central region into the neighbouring pericentromeric region but not the others of heterochromatic region in these cells.

CENP-A^{Cnp1} mis-propagation into the pericentromeric domain results in the expansion of the kinetochore domain

Centromeres associated with the spindle pole body and CENP-A^{Cnp1} form a single focus in the nucleus. Ectopic CENP-A^{Cnp1} propagation into the pericentromeric domain, however, leads to the expansion of nuclear CENP-A^{Cnp1} foci ([42]). To investigate whether these CENP-A^{Cnp1} foci similarly expand in *sfh1-13* mutant cells, we constructed strains expressing GFP-CENP-A^{Cnp1} and Sad1-DsRed from their native promoters and examined their size (Figure 2A). 20% of *sfh1-13* cells had a CENP-A^{Cnp1} foci that were 1.5-times larger than the average size of foci found in wild-type cells, consistent with the observed expansion of CENP-A^{Cnp1} at the pericentromeric region (Figure 1A and B). The spindle pole body-associated protein Sad1 similarly formed foci of a larger size in *sfh1-13* compared with wild-type cells (32% of cells; Figure 2A). Importantly, the majority of cells with enlarged GFP-CENP-A^{Cnp1} foci also exhibited enlarged Sad1-DsRed foci (64%). These data suggest that abnormal CENP-A^{Cnp1} spreading causes an expansion of the kinetochore domain. Since CENP-A chromatin provides a platform for the recruitment of kinetochore proteins to the centromere ([2]), we speculated that ectopic CENP-A^{Cnp1} chromatin on the pericentromere might recruit kinetochore proteins. To examine this hypothesis, we constructed strains expressing myc- or FLAG-tagged CENP-C^{Cnp3}, CENP-I^{Mis6}, Mis16 and HJURP^{Scm3}, and performed ChIP analysis in wild-type and *sfh1-13* mutant backgrounds. In *sfh1-13* mutant cells, a small but significant increase in the localization of CENP-C^{Cnp3} and CENP-I^{Mis6} was observed at surrounding pericentromeric repeats (Figure 2B and C); however, this was not the case for Mis16 or HJURP^{Scm3} (Figure 2D and E), indicating that ectopic CENP-A^{Cnp1} chromatin recruits CENP-C^{Cnp3} and CENP-I^{Mis6} to pericentromeric regions. Taken together, these findings suggest that Sfh1/RSC prevents the propagation of inappropriate kinetochore domains, containing CENP-A^{Cnp1} and associated kinetochore proteins, at the pericentromeric heterochromatin domain.

Clr3/SHREC is required for ectopic deposition of CENP-A^{Cnp1} at the pericentromere

Misloading of CENP-A^{Cnp1} was restricted to pericentromeric heterochromatin, and CENP-A^{Cnp1} did not propagate into neighbouring euchromatic regions (Figure 1A),
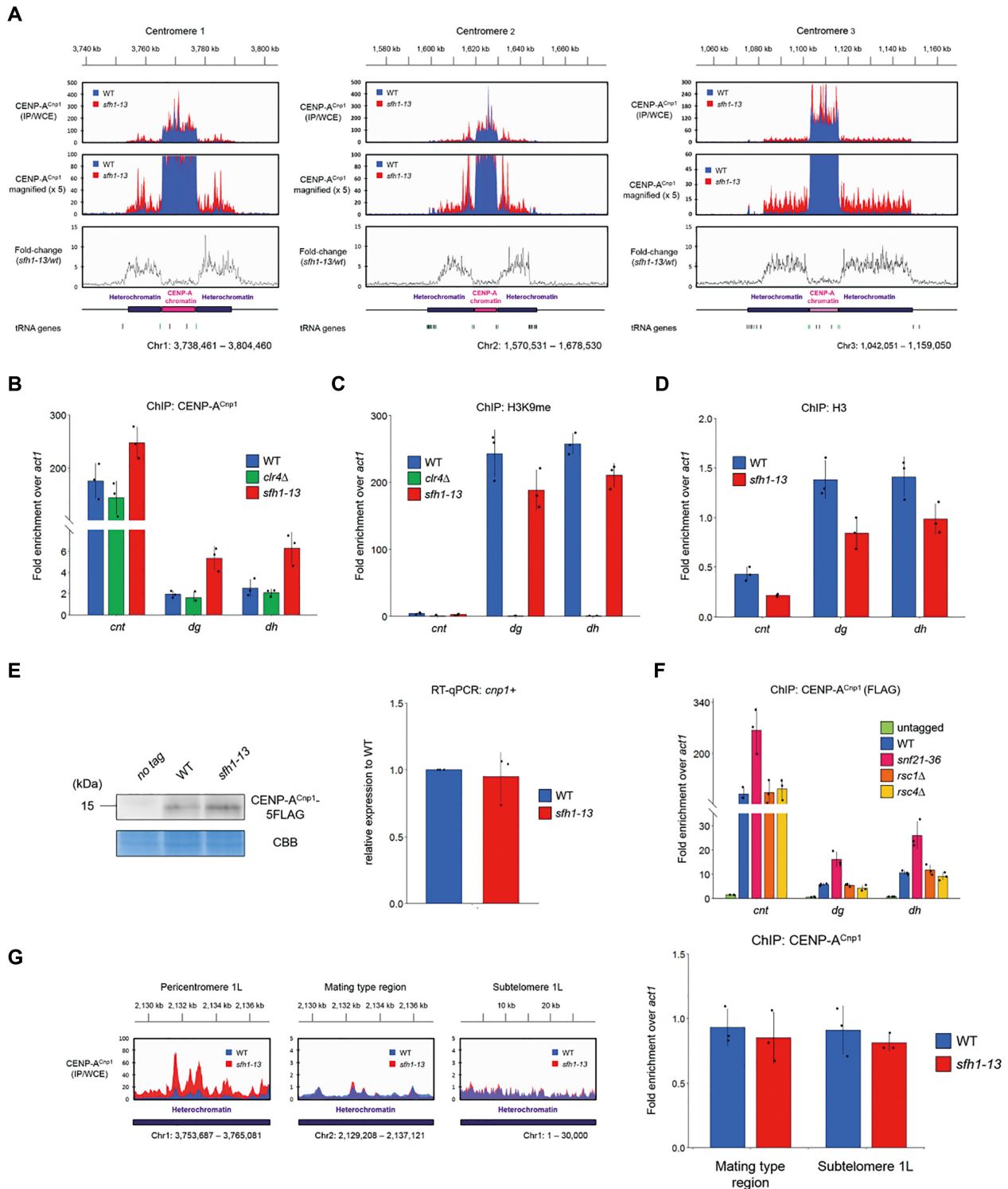
Figure 1. Ectopic CENP-A^{Cnp1} specifically deposits at pericentromeric heterochromatin in RSC-deficient cells. (**A**) ChIP-seq analyses of CENP-A^{Cnp1} around centromere 1, 2 and 3. IP/WCE indicates the tag counts of the immunoprecipitated signal divided by those of whole cell extract. A schematic of the chromatin structure of centromeres is provided at the bottom. Top panels show the distributions of CENP-A^{Cnp1} in wt and *sfh1-13* strains. Middle panels are five times magnified version of the top panel. Bottom panels show the *sfh1-13/wt* ratio. (**B–D**) ChIP-qPCR analyses of CENP-A^{Cnp1} (**B**), H3K9me2 (**C**) and H3 (**D**) at *cnt*, *dg* and *dh* in the indicated strains. Primer positions are shown in Supplementary Figure S2B. Error bars represent the SD of biologically independent experiments (*n* = 3). (**E**) Levels of CENP-A^{Cnp1} in the indicated strains, as determined by immunoblotting (left) and RT-qPCR (right). Error bars represent SD resulting from biological triplicates. (**F**) ChIP-qPCR analysis of CENP-A^{Cnp1} at *cnt*, *dg* and *dh* was performed in the indicated strains. Error bars represent the SD of biologically independent experiments (*n* = 3). (**G**) ChIP-seq analyses of CENP-A^{Cnp1} on heterochromatic domains; pericentromere 1L, the mating-type region and the subtelomere region (left). ChIP-qPCR analysis of CENP-A^{Cnp1} at the mating-type and subtelomere regions was performed in the indicated strains. Error bars represent the SD of biologically independent experiments (*n* = 3) (right).
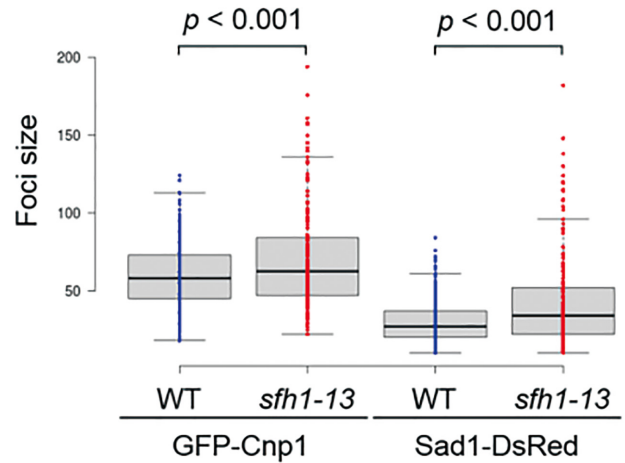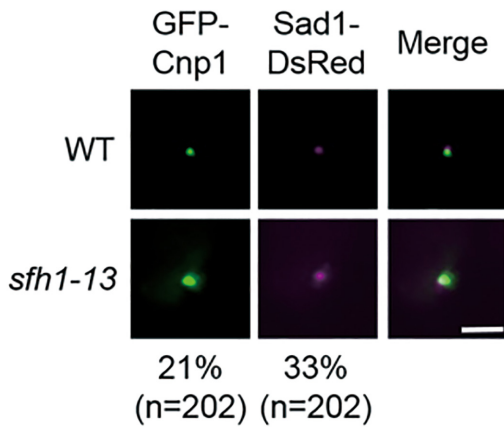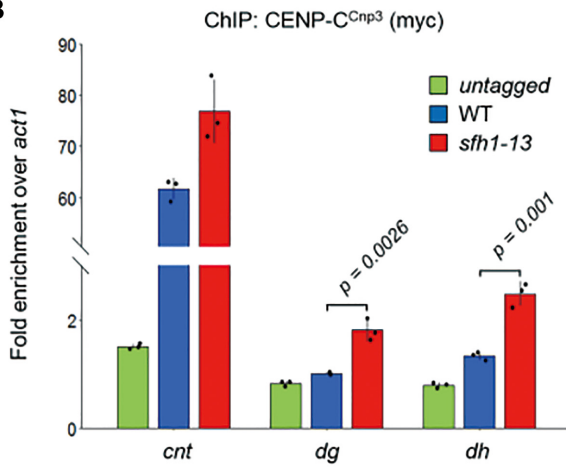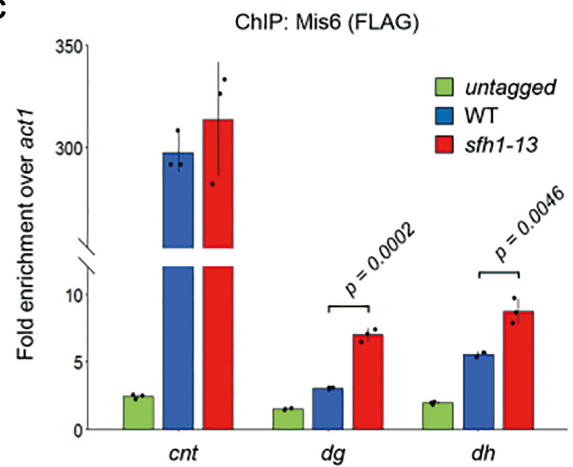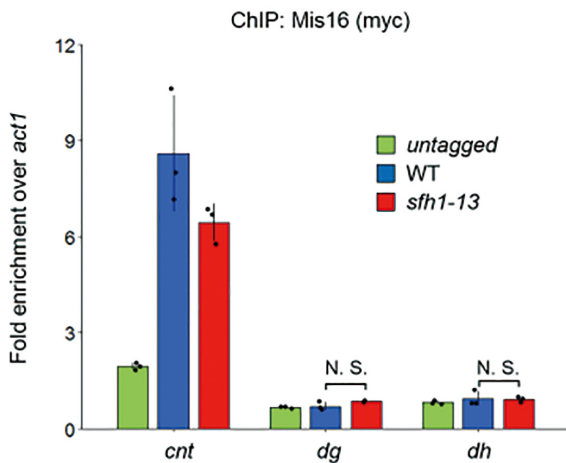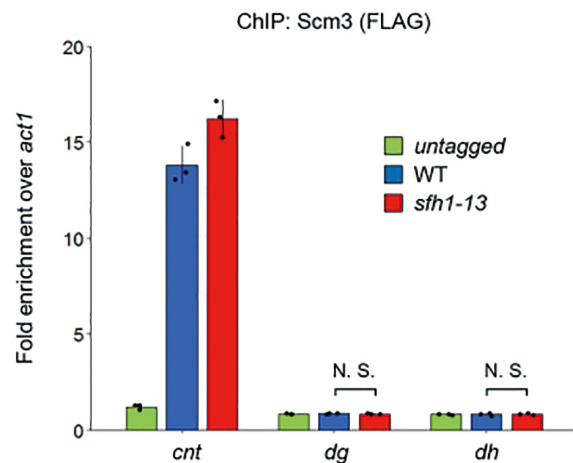
Figure 2. *sfh1-13* mutation induces the abnormal distribution of kinetochore proteins at pericentromere. (**A**) Visualization of CENP-A^{Cnp1} and Sad1 in the nucleus. Wild-type and *sfh1-13* cells expressing GFP-CENP-A^{Cnp1} and Sad1-DsRed were cultured for 6 h at 36°C. Values at the bottom indicate the proportion of cells with CENP-A^{Cnp1} or Sad1 foci ≥50% larger than wild type. Scale bar, 2 μm (left). Boxplot shows the size of CENP-A^{Cnp1} and Sad1 foci in wild-type and *sfh1-13* mutant cells containing a single GFP or DsRed spot (right). (**B–E**) ChIP-qPCR analysis of CENP-C^{Cnp3}, Mis6, Mis16, and Scm3 at *cnt*, *dg* and *dh* in the indicated strains. Enrichment relative to the control *act1* locus is shown on the Y-axis. Error bars represent the SD of biologically independent experiments ($n = 3$). *P*-value was calculated by two-sided Student's *t*-test. N.S., not significant (*P*-value > 0.05).
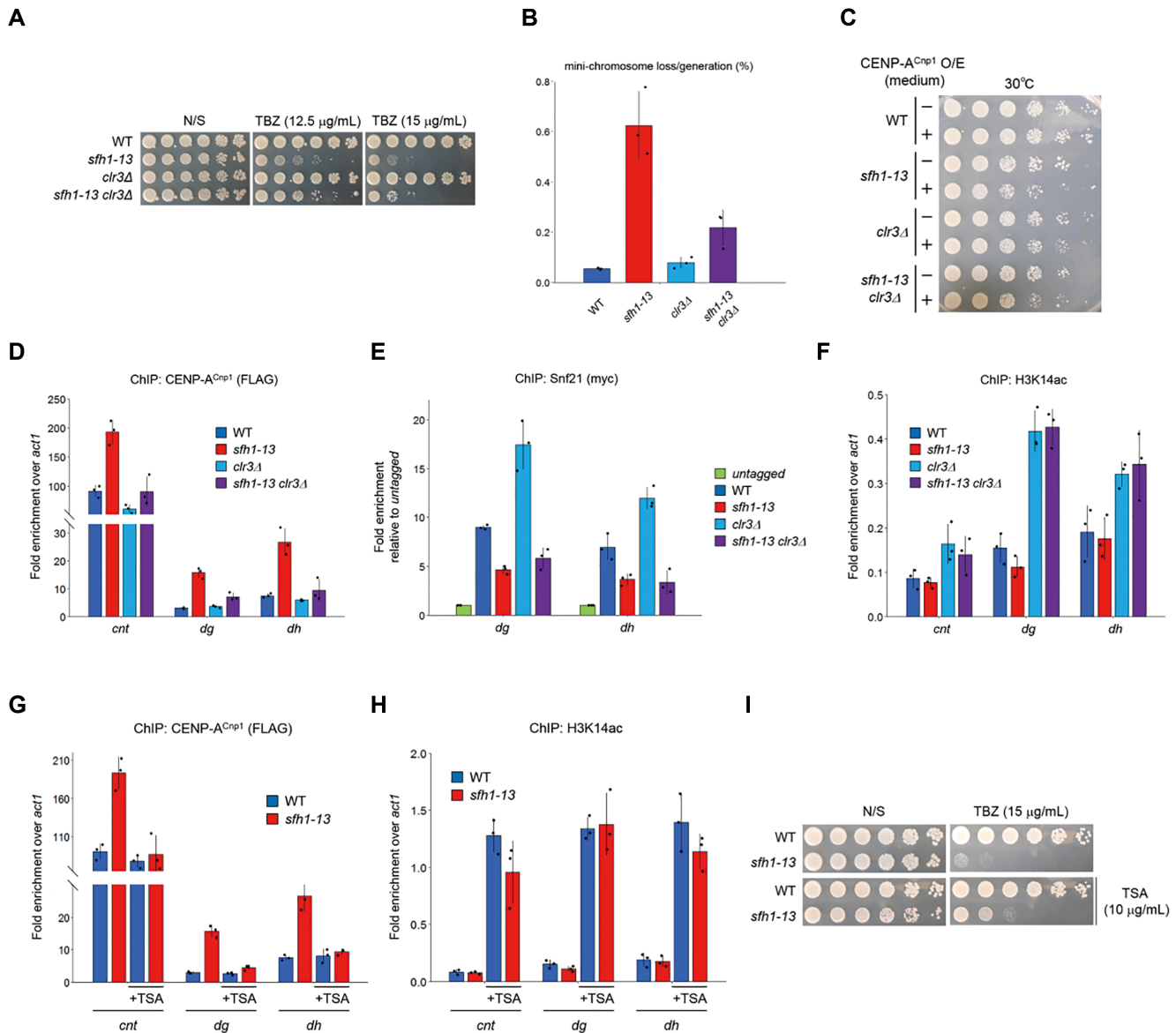
Figure 3. Histone acetylation improves centromeric function and eliminates misloaded CENP-A^{Cnp1} at pericentromere in *sfh1-13* mutant cells. (**A**) TBZ sensitivity of the indicated strains. Each strain was spotted onto the indicated plates and incubated at 30°C for 5 days. (**B**) Minichromosome loss assay monitoring the rate of loss of an artificial chromosome during cell division. Each strain was cultured at the non-permissive temperature for 8 h, and the rate of loss was measured. (**C**) Sensitivity to CENP-A^{Cnp1}-overexpression from the *nmt41* promoter. Cells were grown for 3 days at 30°C. (**D**) ChIP-qPCR analyses of CENP-A^{Cnp1} at *cnt*, *dg* and *dh* in the indicated strains, respectively. Error bars represent the SD of biologically independent experiments (*n* = 3). (**E**) ChIP-qPCR analysis of Snf21-13myc at *dg* and *dh* in the indicated strains. Enrichment relative to an untagged control is shown on the Y-axis. Error bars represent the SD of biologically independent experiments (*n* = 3). (**F**) ChIP-qPCR analyses of H3K14ac at *cnt*, *dg* and *dh* in the indicated strains, respectively. Error bars represent the SD of biologically independent experiments (*n* = 3). (**G and H**) ChIP-qPCR analyses of CENP-A^{Cnp1} (**G**) and H3K14ac (**H**) at *cnt*, *dg* and *dh* was performed in the indicated strains. These strains were preincubated for 8 h with or without TSA (5 μg/ml). Error bars represent the SD of biologically independent experiments (n = 3). The values of WT and *sfh1-13* without TSA are the same as those used in (D and F). (**I**) TBZ sensitivity of the indicated strains with or without TSA (10 μg/ml). Each strain was spotted onto the indicated plates and incubated at 30°C for 3 days.

suggesting that some characteristic of heterochromatin is required for misloading. Heterochromatin contains hypoacetylated histones, which strongly correlate with transcriptional silencing. Histone acetylation levels are associated with CENP-A^{Cnp1} assembly at the central region, and hypoacetylated central chromatin is essential for CENP-A^{Cnp1} loading (43). Hence, we next analyzed the relationship between acetylation of pericentromeric heterochro-

matin and misloading of CENP-A^{Cnp1}. The fission yeast silencing complex SHREC, which contains the histone deacetylase (HDAC) Clr3, maintains the low levels of histone acetylation at heterochromatin (44). Accordingly, we generated *clr3Δ* single and *sfh1-13 clr3Δ* double mutants, and examined their TBZ sensitivity (Figure 3A). *sfh1-13 clr3Δ* cells were faster growing on TBZ-containing plates than *sfh1-13* cells, indicating that deletion of *clr3* partially

rescues the TBZ sensitivity of *sfh1-13*. To confirm whether this phenotype is associated with centromeric function, we next measured the rate of minichromosome loss at the non-permissive temperature. As observed previously, *sfh1-13* exhibited an elevated rate of minichromosome loss, while both *clr3∆* and *sfh1-13 clr3∆* cells maintained minichromosomes (Figure 3B). These results indicate that loss of Clr3 rescues the chromosome segregation defect of *sfh1-13*. Consistently, *sfh1-13 clr3∆* cells were able to tolerate CENP-A^{Cnp1} over-expression, to a greater extent than *sfh1-13* cells (Figure 3C).

Next, we examined CENP-A^{Cnp1} loading by ChIP analysis in *sfh1-13 clr3∆* double mutant cells. *clr3∆* cells did not exhibit ectopic accumulation of CENP-A^{Cnp1} at pericentromeric heterochromatin, while loss of Clr3 eliminated CENP-A^{Cnp1} accumulation at the pericentromere in a *sfh1-13* mutant background, indicating that Clr3 is required for ectopic deposition of CENP-A^{Cnp1} (Figure 3D).

Previously, it was shown that mutation of *clr3* increases centromeric occupancy of Snf21, a catalytic subunit of RSC, suggesting that HDAC activity restricts RSC recruitment to centromeres (45). This effect is due to the binding of RSC to acetylated H3K14 (H3K14ac) (46,47), the level of which is increased in *clr3* mutant cells. Therefore, we hypothesized that the increase in Snf21, induced by loss of Clr3, could eliminate ectopic CENP-A^{Cnp1} at pericentromeres in *sfh1-13∆ clr3∆* cells. To test this possibility, we analyzed centromeric localization of Snf21-13myc by ChIP analysis (Figure 3E). As reported previously, deletion of *clr3* increased the loading of Snf21 at pericentromeric repeats; however, we did not observe greater Snf21 occupancy in our *sfh1-13 clr3∆* double mutant relative to a *sfh1-13* single mutant, suggesting that *sfh1-13* prevents the acetylation-dependent recruitment of Snf21 at pericentromeres, and that the elimination of misloaded CENP-A^{Cnp1} in *sfh1-13∆ clr3∆* cells is not due to the increase in Snf21 level.

Because the deletion of *clr3* increased the acetylation of histones H3 and H4 at the pericentromeric repeats (33,44), we speculated that histone acetylation inhibits ectopic deposition of CENP-A^{Cnp1} at pericentromeres. Analysis of H3K14ac, a target for Clr3/SHREC, revealed that *sfh1-13* cells maintain low levels of H3K14ac at pericentromeric repeats (Figure 3F), indicating that a change in H3K14ac level is not responsible for the misloading of CENP-A^{Cnp1} in the absence of Sfh1/RSC. *sfh1-13 clr3∆* cells exhibited an increase in H3K14ac similar to that observed in *clr3∆* cells (Figure 3F), supporting our hypothesis. To further confirm our hypothesis, we examined, by ChIP analysis, the loading of CENP-A^{Cnp1} in *sfh1-13* cells in the presence of the HDAC inhibitor TSA (Figure 3G and H). TSA treatment did not affect the level of CENP-A^{Cnp1} at pericentromeric heterochromatin in wild-type cells, but it did decrease the accumulation of CENP-A^{Cnp1} at pericentromere in *sfh1-13* cells. Consistent with these results, the addition of TSA partially rescues the TBZ sensitivity of *sfh1-13* cells (Figure 3I). Together, these results suggest that histone deacetylation is a prerequisite for the ectopic deposition of CENP-A^{Cnp1} at pericentromeres, which is suppressed by Sfh1/RSC. Note that at the central domain, deletion of *clr3* or TSA treatment did not affect the CENP-A^{Cnp1} level, though only TSA

treatment caused the elevation of acetylation level. We assume that there is a system that maintains CENP-A^{Cnp1} levels independently on histone acetylation at this region.

Pericentromeric transcription and ectopic deposition of CENP-A^{Cnp1}

Previous studies have revealed that centromeric transcription is vital for CENP-A chromatin assembly. Ino80 and Hrp1, chromatin remodelers with helicase/ATPase activity, are required for regulation of transcription and incorporation of CENP-A^{Cnp1} at the central core region (22,48,49). Transcription at the central region, facilitated by these remodelers, removes histone H3 and, consequently, promotes CENP-A^{Cnp1} deposition. Furthermore, it has been suggested that RNAPII stalling is required for CENP-A^{Cnp1} deposition (50). Taken together, these findings imply that the unique transcriptional environment at the central core domain provides optimal conditions for CENP-A deposition. We next investigated whether Sfh1/RSC regulates transcription in pericentromeric heterochromatin to prevent ectopic CENP-A^{Cnp1} deposition, testing the effect of the *sfh1-13* mutation on centromeric transcription. We found that in wild-type cells, pericentromeric transcripts were undetectable due to transcriptional silencing mediated by the repression of RNAPII recruitment (Supplementary Figure S6A and B). The *sfh1-13* mutation did not affect transcription or RNAPII recruitment, confirming our previous observation that Sfh1/RSC is dispensable for silencing at heterochromatin (12) (Supplementary Figure S6A and B). These data suggest that a simple increase or decrease in RNAPII-dependent transcription does not induce the deposition of CENP-A^{Cnp1} in *sfh1-13* cells. Deletion of *clr3* caused an increase in pericentromeric transcription (Supplementary Figure S6A and B), while pericentromeric transcription and RNAPII recruitment were similarly increased in *sfh1-13 clr3∆* double mutant cells, though to a lesser extent (Supplementary Figure S6A and B). The reduction in transcription in *sfh1-13 clr3∆* cells suggests that Sfh1/RSC contributes to the induction of transcription in the absence of Clr3. Therefore, it is possible that an increase in transcription due to loss of Clr3/SHREC causes the elimination of misloaded CENP-A^{Cnp1} in *sfh1-13* cells. However, it is hard to determine which of these factors is primarily responsible for the elimination of CENP-A^{Cnp1} upon loss of Clr3/SHREC, as hyper-acetylation is tightly coupled with active transcription.

Active transcriptional units substitute for Sfh1/RSC to prevent mis-propagation of CENP-A^{Cnp1} at the boundary

The absence of ectopic deposition of CENP-A^{Cnp1} at the mating-type and telomeric heterochromatin (Figure 1G) suggested that CENP-A^{Cnp1} chromatin spreads over the boundaries into pericentromeric heterochromatin in the absence of Sfh1/RSC, and it is possible that Sfh1/RSC is required for the establishment of the boundaries between the CENP-A^{Cnp1} domain and heterochromatin. At centromere 1 (*cen1*), a 700 bp transition zone that includes two transfer RNA (tRNA) genes is suggested to have sequence-specific
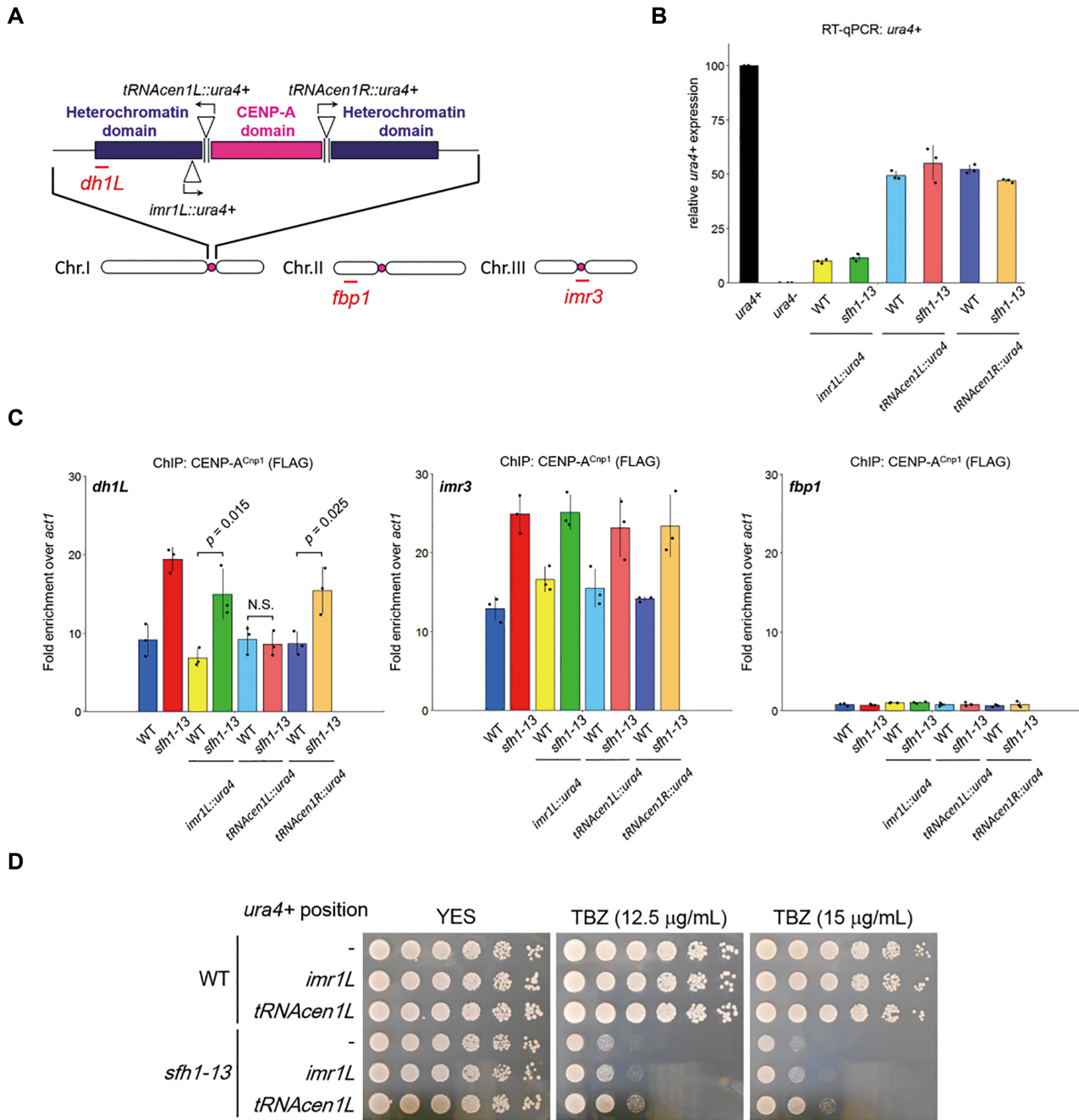
Figure 4. Active transcription at the boundary between two centromeric domains prevents the propagation of ectopic CENP-A[Cnp1] in *sfh1-13* mutant cells. (**A**) Schematic of all chromosomes with an inset detailed view of cen1 showing the insertion sites of an *ura4+* reporter. Pink and purple rectangles indicate the CENP-A[Cnp1] and pericentromeric heterochromatin domain, respectively. Triangles indicate the insertion position of *ura4+*. Vertical black lines indicate the positions of tRNA genes. Horizontal red lines indicate the *dh1L* (on Chr.I), *fbp1* (on Chr.II) and *imr3* (on Chr.III) site for ChIP-qPCR, respectively. (**B**) *ura4+* transcription analysed by RT-qPCR using RNA prepared from the indicated strains. Transcription of the *ura4+* reporter gene in the indicated strains compared with native *ura4+* expression in the wild-type strain are shown on the Y-axis. (**C**) ChIP-qPCR analysis of CENP-A[Cnp1]-5FLAG at *dh1L* (left), *imr3* (middle) and *fbp1* (right) in the indicated strains. Error bars represent the SD of biologically independent experiments ($n = 3$). *P*-value was calculated by two-sided Student's *t*-test. N.S., not significant (*P*-value > 0.05). (**D**) TBZ sensitivity of the indicated strains. Each strain was spotted onto the indicated plates and incubated at 30°C for 3 days.
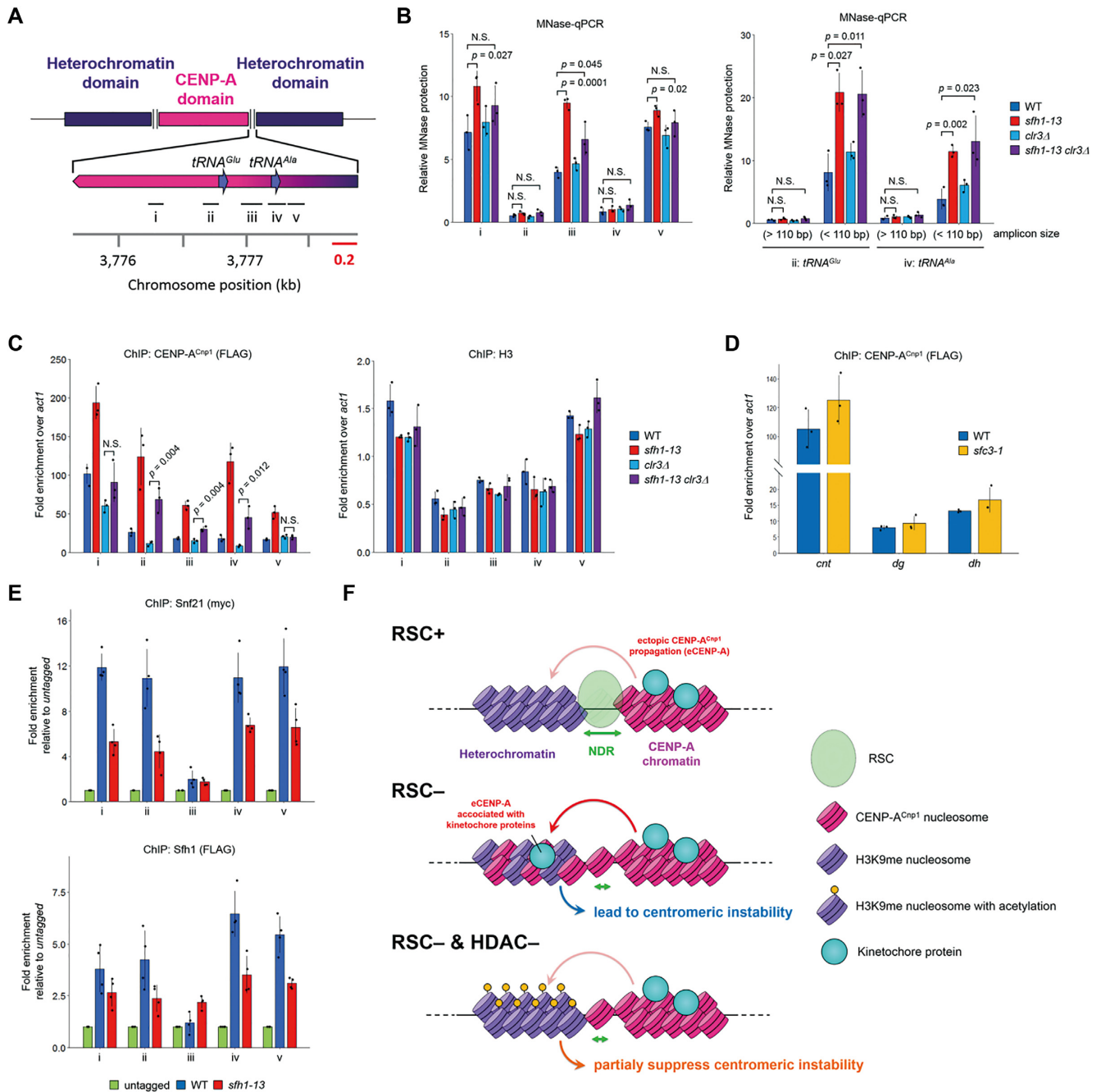
Figure 5. Sfh1/RSC promotes the decompaction of chromatin at the centromeric boundary. (**A**) Schematic structure of centromere 1, with an inset detailed view of the boundary region. Black bars indicate target sites of MNase and ChIP-qPCR. (**B**) MNase-qPCR analysis around the structural transition zone of centromeric chromatin in centromere 1 in the indicated strains. (left) The ratio of MNase-treated and untreated DNA normalized against the *act1* transcriptional termination site (TTS) to determine relative MNase protection. (right) MNase-qPCR analysis at *tRNA^Glu* and *tRNA^Ala* in centromere 1 in the indicated strains. The values of (>110 bp) at *tRNA^Glu* and *tRNA^Ala* are the same as those used in (left). (**C**) ChIP-qPCR analyses of CENP-A^Cnp1-5FLAG (left) and H3 (right) in the indicated strains at five different sites in (sites 1 and 5) or close to (sites 2–4) the boundary is shown on the Y-axis. (**D**) ChIP-qPCR analysis of CENP-A^Cnp1 at *cnt*, *dg* and *dh* was performed in the indicated strains. (**E**) ChIP-qPCR analyses of Snf21-13myc (upper) and 3FLAG-Sfh1 (bottom) in the indicated strains at five different centromeric sites. Enrichment relative to an untagged control is shown on the Y-axis. Error bars represent the SD of biologically independent experiments (*n* = 4). *P*-value was calculated by two-sided Student's *t*-test. N.S., not significant (*P*-value > 0.05). (**F**) A model of centromeric boundary. (Upper) WT cell: RSC promotes the NDR formation at boundary between CENP-A^Cnp1 chromatin and pericentromeric heterochromatin domains. This NDR function preventing ectopic CENP-A^Cnp1 propagation into pericentromere. Therefore, the inappropriate deposition of CENP-A^Cnp1 does not occur in pericentromere in WT cells. (Middle) RSC-deficient cell: RSC defect causes the ectopic CENP-A^Cnp1 deposition/chromatin compaction at the boundary. The details of mechanism are unknown, however, this status attracts a inducing of CNEP-A^Cnp1 propagation associated with some kinetochore proteins into pericentromere resulting that causes the disturbance of centromeric function. (Bottom) RSC and HDAC-deficient cell: the lacking of HDAC or addition of TSA cause histone hyperacetylation in pericentromeric domains. Although ectopic CENP-A^Cnp1 deposition does not eliminate at the boundary, eliminates in pericentromere by this hyperacetylation. Consequently, pericentromeric integrity partially restore to the normal and partially supress the centromeric instability.

chromatin boundary activity (51,52). Recent studies have revealed that transcription plays a role in the formation of chromosomal subdomain boundaries on a fine genome scale (53). In particular, genes that are both long and active are effective as boundary elements to physically separate neighbouring chromosomal domains (54). We hypothesized that if Sfh1/RSC functions at these boundaries, the introduction of a transcription unit at the boundary would reduce the amount of ectopic CENP-A^{Cnp1} spreading in *sfh1-13* cells in *cis*. To examine this, we employed strains that have a *ura4+* reporter between *tRNA^{Glu}* and *tRNA^{Ala}* genes that locates at the left or right side of centromere 1 (*tRNAcen1L/R::ura4+*; Figure 4A). Reporter genes inserted at this position in wild-type cells are stably transcribed and do not affect centromere integrity in *trans* (Supplementary Figure S7) or chromosome segregation (55). We confirmed that this reporter was actively transcribed in both wild-type and *sfh1-13* cells (Figure 4B), before examining whether the reporter could prevent ectopic CENP-A^{Cnp1} deposition. To examine the differential effects of the inserted reporter gene on ectopic CENP-A^{Cnp1} deposition at the left-hand *dh* repeat of centromere 1, we designed the specific primer set (*dh1L*; Figure 4A) that specifically detects the left-hand *dh1* repeat but no other *dh* repeats. In wild-type cells, CENP-A^{Cnp1} localization was unaffected by a *ura4+* reporter inserted either to the left or right of the central domain (*wt tRNAcen1L/R::ura4+*; left panel of Figure 4C). In *sfh1-13* cells, CENP-A^{Cnp1} at the left-hand *dh* repeat was increased. Intriguingly, insertion of *ura4+* to the left of the central domain reduced the CENP-A^{Cnp1} localization (*sfh1-13 tRNAcen1L::ura4+*; left panel of Figure 4C), while insertion at the right did not (*sfh1-13 tRNAcen1R::ura4+*; left panel of Figure 4C). In addition, insertion of the *ura4+* reporter in *cen1* centromere had no effect on CENP-A^{Cnp1} at the pericentromere of *cen3* and the gene-body of *fbp1* as a positive and negative control region, respectively in *sfh1-13* cells (middle and right panel of Figure 4C). We next examined the effect that insertion of the reporter at the outside of the boundary had on CENP-A^{Cnp1} spreading. *imr1L::ura4+* is in a heterochromatin region 415 bp away from *tRNAcen1L::ura4* (Figure 4A). Transcription of the reporter at this heterochromatin locus was repressed (Figure 4B). In this strain, the ectopic deposition of CENP-A^{Cnp1} at left-side *dh* in *cen1* was unaffected in *sfh1-13* cells (left panel of Figure 4C), showing that *ura4+* insertions at this site did not prevent mis-propagation of CENP-A^{Cnp1} in these cells. Importantly, consistent with these results, the *ura4* insertion partially rescues the TBZ sensitivity of *sfh1-13* mutant (Figure 4D). It is surprising that *tRNAcen1L::ura4+* rescued TBZ sensitivity even though it rescued the mis-propagation of CENP-A^{Cnp1} at only one of total six pericentromeric regions. Since chromosome 1 is the largest chromosome but has the smallest pericentromere among three chromosomes, we suspect the defects of the pericentromere of chromosome 1 most contributes to the TBZ sensitivity of the cells. These results suggest that Sfh1/RSC functions at the boundaries to prevent CENP-A^{Cnp1} from spreading into neighbouring heterochromatin, and active transcription can substitute for Sfh1/RSC-dependent boundary activity.

Sfh1/RSC induces a chromatin decompaction at the centromeric boundary

In heterochromatic gene silencing-defective mutants, NDR, formed by RSC, appear at the boundary between the central domain and heterochromatin (33,45). Furthermore, active transcription generally reduces the compaction of chromatin. Therefore, we hypothesized that Sfh1/RSC reduces chromatin compaction at the boundary to prevent improper CENP-A^{Cnp1} propagation into the pericentromeric region. To examine this hypothesis, we performed MNase treatment followed by qPCR (MNase-qPCR) to measure the level of chromatin compaction (Supplementary Figure S8A). To validate this method, we examined whether it was able to detect the NDR known to reside at the transcriptional termination site (TTS) of *act1* (33). We observed a reduction in protection against MNase digestion at the TTS, relative to the gene body, in both wild-type and *sfh1-13* cells (Supplementary Figure S8B), thus we used *act1* TTS as an internal control region. Next, we examined MNase sensitivity at the boundary between the central domain and heterochromatin on chromosome 1 (sites i–v in Figure 5A). In wild-type cells, at sites i and v, MNase protection was 7-fold greater than at the *act1* TTS (left panel of Figure 5B and Supplementary Figure S8B), while sites iii, which correspond to mid-zone of the boundary (Figure 5A), showed a lower-level protection than sites i and v (left panel of Figure 5B). In addition, sites ii and iv, which correspond to tRNA genes (Figure 5A), showed a similar level protection to *act1* TTS (left panel of Figure 5B and Supplementary Figure S8B). These results indicate that the chromatin structure is de-compacted at sites ii, iii and iv, as previously reported (33). Consistent with these results, the levels of CENP-A^{Cnp1} and H3 were relatively low at sites ii, iii, and iv compared with the surrounding region (Figure 5C). Importantly, MNase protection at sites i, iii, and v, which are located between CENP-A^{Cnp1} and heterochromatin domains, was elevated in *sfh1-13* cells (site i: 1.5-fold, *P*-value = 0.027; site iii: 2.2-fold, *P*-value = 0.0001; site v: 1.2-fold, *P*-value = 0.02; left panel of Figure 5B), indicating that Sfh1/RSC contributes to chromatin decompaction at the boundary. We further detected an increase in CENP-A^{Cnp1}, but not in histone H3, present at the boundary region in *sfh1-13* cells (Figure 5C), supporting the idea that CENP-A^{Cnp1} spreads over the boundary in the absence of Sfh1/RSC. Interestingly, in *sfh1-13 clr3Δ* cells, the chromatin compaction in the boundary region observed in the *sfh1-13* cells was partly suppressed (site i, iii and v; left panel of Figure 5B). Consistent with this, the level of CENP-A^{Cnp1} reduced in *sfh1-13 clr3Δ* cells compared with that of *sfh1-13* cells (Figure 5C). However, *sfh1-13 clr3Δ* cells maintained higher levels of CENP-A^{Cnp1} than *clr3Δ* cells at the boundary (site ii: 5.8-fold, *P*-value = 0.004; site iii: 2.0-fold, *P*-value = 0.004; site iv: 5.2-fold, *P*-value = 0.012; Figure 5C), indicating that the ectopic CENP-A^{Cnp1} deposition was not completely cancelled at this region in *sfh1-13 clr3Δ* cells. These results suggest that Sfh1/RSC creates the centromeric boundary by forming NDR which is responsible for the prevention of CENP-A^{Cnp1} spread toward the boundary, which is required for the ectopic CENP-A^{Cnp1} deposition at this region even in the absence of Clr3.

While we did not detect a change in MNase protection at tRNA genes in *sfh1-13* cells, we did detect ectopic CENP-A^{Cnp1} deposition (left panel of Figure 5B and C, sites ii and iv). It is possible that these sites are protected from MNase by a non-canonical histone complex, such as CENP-A hemisomes (56), remodeled nucleosomes (57), or RNA Polymerase III (RNAP III) and its transcription factor (TFIIIC), resulting in the production of small DNA fragments by MNase digestion, which was not amplified by our primers (amplicon size: ∼130 bp). Indeed, MNase digestion of the tRNA gene locus has been shown to produce shorter DNA fragments than canonical mono-nucleosomal DNA at fission yeast centromeres (<110 bp) (58). Therefore, we re-examined the MNase digestion products with primers that could detect shorter DNA templates (<110 bp), and observed that MNase protection at sites ii and iv were elevated in *sfh1-13* cells (right panel of Figure 5B), suggesting that Sfh1/RSC defects induce the formation of non-canonical histone complexes containing CENP-A^{Cnp1} at tRNA gene loci.

Previous studies have shown that tRNA genes are located at the transition zones in fission yeast centromeres (59,60), and these loci play a role in chromatin boundary activity (51,52). This raised the possibility that the RNAPIII complex, and/or the transcription of tRNA genes by RNAPIII, are involved in barring improper CENP-A^{Cnp1} propagation. To examine this possibility, we analyzed the effect of the temperature-sensitive *sfc3-1* mutation on CENP-A^{Cnp1} propagation. *sfc3* encodes a subunit of TFIIIC complex that binds to the B box of tRNA gene promoters, and is required for tRNA gene transcription (61). We did not detect ectopic depositions of CENP-A^{Cnp1} at *dg* and *dh* in *sfc3-1* cells at semi-permissive temperatures (Figure 5D). Therefore, we concluded that RNAPIII complex and its transcription are not involved in the prevention of ectopic CENP-A^{Cnp1} propagation.

Finally, to examine whether RSC acts directly at boundaries, we performed ChIP analyses on wild-type and *sfh1-13* cells expressing tagged Snf21 and Sfh1. Previous ChIP-sequencing results of Snf21 study showed that relatively higher levels of Snf21 localized at the boundary between the center region and heterochromatint (62). Consistent with this, we found that Snf21 and Sfh1 were enriched across the boundary of centromere 1 in wild-type cells (Figure 5E). These distributions phenocopy the distribution of RSC around promoters, where RSC maintains NDR (63). Furthermore, we observed a ∼50% reduction in Snf21 and Sfh1 in *sfh1-13* cells compared with wild-type cells at all test sites. These results suggest that RSC directly interferes with chromatin compaction at the boundary.

DISCUSSION

Our findings demonstrate that defects in RSC cause ectopic deposition of CENP-A^{Cnp1} at pericentromeric but not telomeric or mating-type locus heterochromatin. We also observed some increase of CENP-A^{Cnp1} at the central region in *sfh1-13* cells, which may be the primary cause of the expansion of CENP-A^{Cnp1} to pericentromeric heterochromatin. However, we think it is unlikely by the following rea-

sons. We confirmed that the ectopic deposition occurs at the out-most region of pericentromere (Figure 1A and 4C), which may not be explained by the increase of CENP-A^{Cnp1} at the central region. Furthermore, in the previous study, the increase of CENP-A^{Cnp1} at pericentromeric region was marginal, even when the strong overexpression of CENP-A^{Cnp1} causes a large increase in CENP-A^{Cnp1} in the central region (23).

One possibility is that RSC evicts misloaded CENP-A^{Cnp1} from pericentromeric heterochromatin; however, RSC localizes to CENP-A^{Cnp1} chromatin but does not evict CENP-A^{Cnp1} nucleosome (12), and insertion of *ura4+* at one of the boundaries inhibited the ectopic accumulation of CENP-A^{Cnp1} in *cis* in RSC-deficient cells. Furthermore, we have shown the ectopic CENP-A^{Cnp1} accumulation at the boundary even in *sfh1-13 clr3Δ* cells compared with *clr3Δ* cells though CENP-A^{Cnp1} level at the central region was not changed in both cells (Figure 5C). This suggests that RSC suppress CENP-A^{Cnp1} expansion at the boundary independently on Clr3 function or increase of CENP-A^{Cnp1} at the central region. Thus, we conclude that Sfh1/RSC prevents the spread of CENP-A^{Cnp1} chromatin from the central domain into the neighbouring pericentromeric domain at the boundaries (Figure 5F).

Previous studies have reported that ectopic CENP-A deposition often occurs at heterochromatin (22,23,42). In the present study, we have shown that hypoacetylated histones at heterochromatin are required for CENP-A^{Cnp1} spreading (Figure 3D and G). This is consistent with a previous report suggesting that Mis16- and Mis18-dependent deacetylation of histones at the central domain is required for CENP-A^{Cnp1} assembly at this region (43). However, we do not have a detailed mechanism for CENP-A^{Cnp1} mis-propagation. Mis16 and HJURP^{Scm3}, which are required for loading of CENP-A^{Cnp1} at the centromeric core region (64), did not mis-propagate with CENP-A^{Cnp1} in *sfh1-13* cells (Figure 2D and E), suggesting both proteins are not involved in CENP-A^{Cnp1} mis-propagation. In addition, we did not observe transcriptional activation, which can induce the exchange of histone H3 for CENP-A^{Cnp1}, in *sfh1-13* cells (Supplementary Figure S6B). These results suggest that the CENP-A^{Cnp1} propagation at pericentromere differs from conventional propagation at the core region. We have shown that mis-propagated CENP-A^{Cnp1} recruits a subset of kinetochore components, including CENP-C^{Cnp3} and CENP-I^{Mis6}, in the absence of Sfh1/RSC function (Figure 2B and C), which could cause chromosome segregation defects. Furthermore, this suggest that mis-propagated CENP-A^{Cnp1} retains some function, though we do not know whether it is incorporated in the nucleosome at this stage. Therefore, preventing CENP-A^{Cnp1} mis-propagation at the boundaries between central CENP-A^{Cnp1} domains and pericentromeric heterochromatin is crucial for the function of centromeres.

Previous studies have reported that chromatin decompaction blocks the propagation of specific chromatin states by separating neighbouring nucleosomes (65). For example, both (CCGNN)$_n$ and poly(dA-dT) sequences, which prevent the formation of nucleosomes, block the spread of heterochromatin in budding yeast (66). Furthermore, tDNAs,

which encode tRNAs, are nucleosome-depleted and function as a barrier to heterochromatin spread in human cells (67). At fission yeast centromeres, tDNAs are constitutive NDRs located at transition zones between CENP-A^{Cnp1} chromatin domains and heterochromatin domains (Figure 5B) (45,51,52,59). Deletion of tDNAs induces the propagation of heterochromatin into CENP-A^{Cnp1} domains but not the propagation of CENP-A^{Cnp1} into heterochromatin (52). In addition, the transcriptional inactivation of tDNAs by *sfc3-1* mutation does not cause mis-propagation of CENP-A^{Cnp1} (Figure 5D). These results indicate that tDNAs function as a barrier to the spread of heterochromatin but not to CENP-A^{Cnp1}. By contrast, loss of Sfh1/RSC causes mis-propagation of CENP-A^{Cnp1} but not heterochromatin. These findings show that Sfh1/RSC establishes a barrier to CENP-A^{Cnp1} propagation at the boundary region independent from the tDNA-based heterochromatin barrier.

RSC mutations cause shrinkage in NDRs throughout the fission yeast genome (17), indicating that RSC participates in chromatin decompaction. Our analyses show that defects in Sfh1/RSC cause partial loss of chromatin decompaction, which appears to be associated with the spread of CENP-A^{Cnp1} over the boundary (Figure 5B and C). Thus, NDRs appear to function as a barrier against CENP-A^{Cnp1} propagation. We have shown that the insertion of *ura4+* at boundaries can block CENP-A^{Cnp1} propagation in the absence of the Sfh1/RSC-dependent barrier (Figure 4C). Since we have shown that the insertion of *ura4+* into neighbouring heterochromatin, where transcription is repressed, has no barrier activity (Figure 4C), we believe that transcription prevents the spread of CENP-A^{Cnp1}. It is possible that active transcription units cause a high level of nucleosome turnover, inducing the decompaction of chromatin, which functions as a barrier to CENP-A^{Cnp1} spread. Previous studies have shown that RSC plays a dominant role in establishing the size of NDRs, which is achieved by preventing an inward shift of the +1 and −1 nucleosomes (13–15). We speculate that the same mechanism separates distinct centromeric domains and maintains the barrier to CENP-A^{Cnp1} mis-propagation at the centromeric boundary. Shrinkage of this boundary when RSC is defective could promote propagation of CENP-A^{Cnp1} into heterochromatic domains (Figure 5F).

Our results reveal a novel function for the RSC-dependent decompaction of chromatin. This improves our understanding of how RSC contributes to chromatin-related processes in the cell, and of the mechanisms responsible for the control of the distribution and size of distinct chromatin domains.

DATA AVAILABILITY

Sequencing raw and processed data have been deposited in DDBJ (https://www.ddbj.nig.ac.jp/index-e.html) with the accession number DRA007530 and E-GEAD-471, respectively.

SUPPLEMENTARY DATA

Supplementary Data are available at NAR Online.

REFERENCES

1. Black,B.E., Foltz,D.R., Chakravarthy,S., Luger,K., Woods,V.L. and Cleveland,D.W. (2004) Structural determinants for generating centromeric chromatin. *Nature*, **430**, 578–582.
2. De Rop,V., Padeganeh,A. and Maddox,P.S. (2012) CENP-A: the key player behind centromere identity, propagation, and kinetochore assembly. *Chromosoma*, **121**, 527–538.
3. Cheeseman,I.M. and Desai,A. (2008) Molecular architecture of the kinetochore-microtubule interface. *Nat. Rev. Mol. Cell Biol.*, **9**, 33–46.
4. Chen,C.C. and Mellone,B.G. (2016) Chromatin assembly: journey to the CENter of the chromosome. *J. Cell Biol.*, **214**, 13–24.
5. Hota,S.K. and Bruneau,B.G. (2016) ATP-dependent chromatin remodeling during mammalian development. *Development*, **143**, 2882–2897.
6. Cao,Y., Cairns,B.R., Kornberg,R.D. and Laurent,B.C. (1997) Sfh1p, a component of a novel chromatin-remodeling complex, is required for cell cycle progression. *Mol. Cell. Biol.*, **17**, 3323–3334.
7. Hsu,J.-M., Huang,J., Meluh,P.B. and Laurent,B.C. (2003) The yeast RSC chromatin-remodeling complex is required for kinetochore function in chromosome segregation. *Mol. Cell. Biol.*, **23**, 3202–3215.
8. Huang,J., Hsu,J.M. and Laurent,B.C. (2004) The RSC nucleosome-remodeling complex is required for cohesin's association with chromosome arms. *Mol. Cell*, **13**, 739–750.
9. Shim,E.Y., Ma,J.-L., Oum,J.-H., Yanez,Y. and Lee,S.E. (2005) The yeast chromatin remodeler RSC complex facilitates end joining repair of DNA double-strand breaks. *Mol. Cell. Biol.*, **25**, 3934–3944.
10. Monahan,B.J., Villén,J., Marguerat,S., Bähler,J., Gygi,S.P. and Winston,F. (2008) Fission yeast SWI/SNF and RSC complexes show compositional and functional differences from budding yeast. *Nat. Struct. Mol. Biol.*, **8**, 873–880.
11. Yamada,K., Hirota,K., Mizuno,K.-I., Shibata,T. and Ohta,K. (2008) Essential roles of snf21, a swi2/snf2 family chromatin remodeler, in fission yeast mitosis. *Genes Genet. Syst.*, **83**, 361–372.
12. Kotomura,N., Tsunemine,S., Kuragano,M., Asanuma,T., Nakagawa,H., Tanaka,K. and Murakami,Y. (2018) Sfh1, an essential component of the RSC chromatin remodeling complex, maintains genome integrity in fission yeast. *Genes Cells*, **23**, 738–752.
13. Badis,G., Chan,E.T., van Bakel,H., Pena-Castillo,L., Tillo,D., Tsui,K., Carlson,C.D., Gossett,A.J., Hasinoff,M.J., Warren,C.L. *et al.* (2008) A library of yeast transcription factor motifs reveals a widespread function for rsc3 in targeting nucleosome exclusion at promoters. *Mol. Cell*, **32**, 878–887.
14. Hartley,P.D. and Madhani,H.D. (2009) Mechanisms that specify promoter nucleosome location and identity. *Cell*, **137**, 445–458.
15. Parnell,T.J., Huff,J.T. and Cairns,B.R. (2008) RSC regulates nucleosome positioning at pol II genes and density at pol III genes. *EMBO J.*, **27**, 100–110.

16. Wippo,C.J., Israel,L., Watanabe,S., Hochheimer,A., Peterson,C.L. and Korber,P. (2011) The RSC chromatin remodelling enzyme has a unique role in directing the accurate positioning of nucleosomes. *EMBO J.*, **30**, 1277–1288.

17. Yague-Sanz,C., Vázquez,E., Sánchez,M., Antequera,F. and Hermand,D. (2017) A conserved role of the RSC chromatin remodeler in the establishment of nucleosome-depleted regions. *Curr. Genet.*, **63**, 187–193.

18. Clapier,C.R., Kasten,M.M., Parnell,T.J., Viswanathan,R., Szerlong,H., Sirinakis,G., Zhang,Y. and Cairns,B.R. (2016) Regulation of DNA translocation efficiency within the chromatin remodeler RSC/Sth1 potentiates nucleosome sliding and ejection. *Mol. Cell*, **62**, 453–461.

19. Sinha,K.K., Gross,J.D. and Narlikar,G.J. (2017) Distortion of histone octamer core promotes nucleosome mobilization by a chromatin remodeler. *Science*, **355**, eaaa3761.

20. Gikopoulos,T., Singh,V., Tsui,K., Awad,S., Renshaw,M.J., Scholfield,P., Barton,G.J., Nislow,C., Tanaka,T.U. and Owen-hughes,T. (2011) The SWI /SNF complex acts to constrain distribution of the centromeric histone variant cse4. *EMBO J.*, **30**, 1919–1927.

21. Mathew,V., Pauleau,A.L., Steffen,N., Bergner,A., Becker,P.B. and Erhardt,S. (2014) The histone-fold protein CHRAC14 influences chromatin composition in response to DNA damage. *Cell Rep.*, **7**, 321–330.

22. Choi,E.S., Stralforss,A., Catania,S., Castillo,A.G., Svensson,J.P., Pidoux,A.L., Ekwall,K. and Allshire,R.C. (2012) Factors that promote H3 chromatin integrity during transcription prevent promiscuous deposition of CENP-ACnp1 in fission yeast. *PLoS Genet.*, **8**, e1002985.

23. Kitagawa,T., Ishii,K., Takeda,K. and Matsumoto,T. (2014) The 19S proteasome subunit rpt3 regulates distribution of CENP-A by associating with centromeric chromatin. *Nat. Commun.*, **5**, 3597.

24. Motamedi,M.R., Hong,E.J.E., Li,X., Gerber,S., Denison,C., Gygi,S. and Moazed,D. (2008) HP1 proteins form distinct complexes and mediate heterochromatic gene silencing by nonoverlapping mechanisms. *Mol. Cell*, **32**, 778–790.

25. Fischer,T., Cui,B., Dhakshnamoorthy,J., Zhou,M., Rubin,C., Zofall,M., Veenstra,T.D. and Grewal,S.I.S. (2009) Diverse roles of HP1 proteins in heterochromatin assembly and functions in fission yeast. *Proc. Natl. Acad. Sci. U.S.A.*, **106**, 8998–9003.

26. Moreno,S., Klar,A. and Nurse,P. (1991) Molecular genetic analysis of fission yeast schizosaccharomyces pombe. *Methods Enzymol.*,**194**, 795–823.

27. Bähler,J., Wu,J.Q., Longtine,M.S., Shah,N.G., McKenzie,A., Steever,A.B., Wach,A., Philippsen,P. and Pringle,J.R. (1998) Heterologous modules for efficient and versatile PCR-based gene targeting in schizosaccharomyces pombe. *Yeast*, **14**, 943–951.

28. Takayama,Y., Sato,H., Saitoh,S., Ogiyama,Y., Masuda,F. and Takahashi,K. (2008) Biphasic incorporation of centromeric histone CENP-A in fission yeast. *Mol. Biol. Cell*, **19**, 682–690.

29. Nakagawa,H., Lee,J.K., Hurwitz,J., Allshire,R.C., Nakayama,J.I., Grewal,S.I.S., Tanaka,K. and Murakami,Y. (2002) Fission yeast CENP-B homologs nucleate centromeric heterochromatin by promoting heterochromatin-specific histone tail modifications. *Genes Dev.*,**16**, 1766–1778.

30. Dohke,K., Miyazaki,S., Tanaka,K., Urano,T., Grewal,S.I.S. and Murakami,Y. (2008) Fission yeast chromatin assembly factor 1 assists in the replication-coupled maintenance of heterochromatin. *Genes Cells*, **13**, 1027–1043.

31. Kawakami,K., Hayashi,A., Nakayama,J.I. and Murakami,Y. (2012) A novel RNAi protein, dsh1, assembles RNAi machinery on chromatin to amplify heterochromatic siRNA. *Genes Dev.*,**26**, 1811–1824.

32. Lantermann,A., Stråfors,A., Fagerström-Billai,F., Korber,P. and Ekwall,K. (2009) Genome-wide mapping of nucleosome positions in schizosaccharomyces pombe. *Methods*, **48**, 218–225.

33. Kato,H., Okazaki,K., Iida,T., Nakayama,J.-I., Murakami,Y. and Urano,T. (2013) Spt6 prevents transcription-coupled loss of posttranslationally modified histone h3. *Sci. Rep.*, **3**, 2186.

34. Li,H. and Durbin,R. (2009) Fast and accurate short read alignment with burrows-wheeler transform. *Bioinformatics*, **25**, 1754–1760.

35. Li,H., Handsaker,B., Wysoker,A., Fennell,T., Ruan,J., Homer,N., Marth,G., Abecasis,G. and Durbin,R. (2009) The sequence alignment/map format and SAMtools. *Bioinformatics*, **25**, 2078–2079.

36. Zhang,Y., Liu,T., Meyer,C.A., Eeckhoute,J., Johnson,D.S., Bernstein,B.E., Nussbaum,C., Myers,R.M., Brown,M., Li,W. *et al.* (2008) Model-based analysis of chip-Seq (MACS). *Genome Biol.*, **9**, R137.

37. Thorvaldsdóttir,H., Robinson,J.T. and Mesirov,J.P. (2013) Integrative genomics viewer (IGV): High-performance genomics data visualization and exploration. *Brief. Bioinform.*, **14**, 178–192.

38. Ekwall,K., Cranston,G. and Allshire,R.C. (1999) Fission yeast mutants that alleviate transcriptional silencing in centromeric flanking repeats and disrupt chromosome segregation. *Genetics*, **153**, 1153–1169.

39. Basi,G., Schmid,E. and Maundrell,K. (1993) TATA box mutations in the schizosaccharomyces pombe nmt1 promoter affect transcription efficiency but not the transcription start point or thiamine repressibility. *Gene*, **123**, 131–136.

40. Castillo,A.G., Mellonea,B.G., Partridgeb,J.F., Richardsonc,W., Hamilton,G.L., Allshire,R.C. and Pidoux,A.L. (2007) Plasticity of fission yeast CENP-A chromatin driven by relative levels of histone H3 and h4. *PLos Genet.,*,**3**, 1264–1274.

41. Hayashi,T., Ebe,M., Nagao,K., Kokubu,A., Sajiki,K. and Yanagida,M. (2014) Schizosaccharomyces pombe centromere protein mis19 links mis16 and mis18 to recruit CENP-A through interacting with NMD factors and the SWI/SNF complex. *Genes Cells*, **19**, 541–554.

42. Gonzalez,M., He,H., Sun,S., Li,C. and Li,F. (2013) Cell cycle-dependent deposition of CENP-A requires the dos1/2-cdc20 complex. *Proc. Natl. Acad. Sci. U.S.A.*, **110**, 606–611.

43. Hayashi,T., Fujita,Y., Iwasaki,O., Adachi,Y., Takahashi,K. and Yanagida,M. (2004) Mis16 and mis18 are required for CENP-A loading and histone deacetylation at centromeres. *Cell*, **118**, 715–729.

44. Sugiyama,T., Cam,H.P., Sugiyama,R., Noma,K.ichi, Zofall,M., Kobayashi,R. and Grewal,S.I.S. (2007) SHREC, an effector complex for heterochromatic transcriptional silencing. *Cell*, **128**, 491–504.

45. Garcia,J.F., Dumesic,P.A., Hartley,P.D., El-Samad,H. and Madhani,H.D. (2010) Combinatorial, site-specific requirement for heterochromatic silencing factors in the elimination of nucleosome-free regions. *Genes Dev.*,**24**, 1758–1771.

46. Wang,Y., Kallgren,S.P., Reddy,B.D., Kuntz,K., López-Maury,L., Thompson,J., Watt,S., Chun,M., Hou,H., Shi,Y. *et al.* (2012) Histone H3 lysine 14 acetylation is required for activation of a DNA damage checkpoint in fission yeast. *J. Biol. Chem.*, **287**, 4386–4393.

47. Duan,M.R. and Smerdon,M.J. (2014) Histone H3 lysine 14 (H3K14) acetylation facilitates DNA repair in a positioned nucleosome by stabilizing the binding of the chromatin remodeler RSC (Remodels structure of chromatin). *J. Biol. Chem.*, **289**, 8353–8363.

48. Walfridsson,J., Bjerling,P., Thalen,M., Yoo,E.J., Park,S.D. and Ekwall,K. (2005) The CHD remodeling factor hrp1 stimulates CENP-A loading to centromeres. *Nucleic Acids Res.,***33**, 2868–2879.

49. Singh,P.P., Shukla,M., White,S.A., Lafos,M., Tong,P., Auchynnikava,T., Spanos,C., Rappsilber,J., Pidoux,A.L. and Allshire,R.C. (2020) Hap2-Ino80-facilitated transcription promotes de novo establishment of CENP-A chromatin. *Genes Dev.*, **34**, 226–238.

50. Catania,S., Pidoux,A.L. and Allshire,R.C. (2015) Sequence features and transcriptional stalling within centromere DNA promote establishment of CENP-A chromatin. *PLos Genet.,*11.

51. Partridge,J.F., Borgstrøm,B. and Allshire,R.C. (2000) Distinct protein interaction domains and protein spreading in a complex centromere. *Genes Dev.*,**14**, 783–791.

52. Scott,K.C., Merrett,S.L. and Willard,H.F. (2006) A heterochromatin barrier partitions the fission yeast centromere into discrete chromatin domains. *Curr. Biol.*, **16**, 119–129.

53. van Steensel,B. and Furlong,E.E.M. (2019) The role of transcription in shaping the spatial organization of the genome. *Nat. Rev. Mol. Cell Biol.*, **20**, 327–337.

54. Le,T.B. and Laub,M.T. (2016) Transcription rate and transcript length drive formation of chromosomal interaction domain boundaries. *EMBO J.*, **35**, 1582–1595.

55. Allshire,R.C., Nimmo,E.R., Ekwall,K., Javerzat,J.P. and Cranston,G. (1995) Mutations derepressing silent centromeric domains in fission yeast disrupt chromosome segregation. *Genes Dev.,***9**, 218–233.

56. Henikoff,S., Ramachandran,S., Krassovsky,K., Bryson,T.D., Codomo,C.A., Brogaard,K., Widom,J., Wang,J.-P. and Henikoff,J.G. (2014) The budding yeast centromere DNA element II wraps a stable cse4 hemisome in either orientation in vivo. *Elife*, **3**, e01861.

57. Biernat,E., Kinney,J., Dunlap,K., Rizza,C. and Govind,C.K. (2021) The RSC complex remodels nucleosomes in transcribed coding sequences and promotes transcription in saccharomyces cerevisiae. *Genetics*, **217**, iyab021.

58. Thakur,J., Talbert,P.B. and Henikoff,S. (2015) Inner kinetochore protein interactions with regional centromeres of fission yeast. *Genetics*, **201**, 543–561.

59. Takahashi,K., Murakami,S., Chikashige,Y., Niwa,O. and Yanagida,M. (1991) A large number of tRNA genes are symmetrically located in fission yeast centromeres. *J. Mol. Biol.*, **218**, 13–17.

60. Takahashi,K., Murakami,S., Chikashige,Y., Funabiki,H., Niwa,O. and Yanagida,M. (1992) A low copy number central sequence with strict symmetry and unusual chromatin structure in fission yeast centromere. *Mol. Biol. Cell*, **3**, 819–835.

61. Iwasaki,O., Tanaka,A., Tanizawa,H., Grewal,S.I.S. and Noma,K.-I. (2010) Centromeric localization of dispersed pol III genes in fission yeast. *Mol. Biol. Cell*, **21**, 254–265.

62. Lee,J., Shik Choi,E., David Seo,H., Kang,K., Gilmore,J.M., Florens,L., Washburn,M.P., Choe,J., Workman,J.L. and Lee,D. (2017) Chromatin remodeller fun30fft3 induces nucleosome disassembly to facilitate RNA polymerase II elongation. *Nat. Commun.*, **8**, 14527.

63. Ramachandran,S., Zentner,G.E. and Henikoff,S. (2014) Asymmetric nucleosomes flank promoters in the budding yeast genome. *Genome Res.*, **25**, 381–390.

64. Williams,J.S., Hayashi,T., Yanagida,M. and Russell,P. (2009) Fission yeast scm3 mediates stable assembly of Cnp1/CENP-A into centromeric chromatin. *Mol. Cell*, **33**, 287–298.

65. Sekulic,N. and Black,B.E. (2009) A reader for centromeric chromatin. *Nat. Cell Biol.*, **11**, 793–795.

66. Bi,X., Yu,Q., Sandmeier,J.J. and Zou,Y. (2004) Formation of boundaries of transcriptionally silent chromatin by nucleosome-excluding structures. *Mol. Cell. Biol.*, **24**, 2118–2131.

67. Raab,J.R., Chiu,J., Zhu,J., Katzman,S., Kurukuti,S., Wade,P.A., Haussler,D. and Kamakaka,R.T. (2012) Human tRNA genes function as chromatin insulators. *EMBO J.*, **31**, 330–350.